Nanoscale

Accepted Manuscript

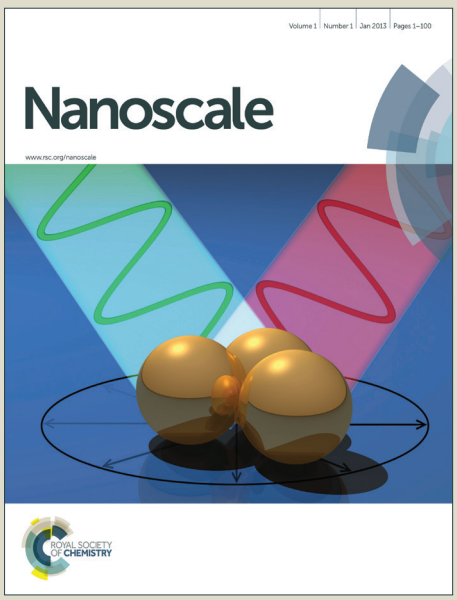

ROYAL SOCIETY OF CHEMISTRY

www.rsc.org/nanoscale

ARTICLE TYPE www. rsc.org/xxxxxx | XXXXXXXX

Layer number identification of intrinsic and defective multilayer graphenes by the Raman mode intensity from substrate

Xiao-Li Li, Xiao-Fen Qiao, Wen-Peng Han, Yan Lu, Qing-Hai Tan, Xue-Lu Liu, and Ping-Heng Tan*

Received Xth XXXXXXXXXX 20XX, Accepted Xth XXXXXXXXX 20XX
First published on the web Xth XXXXXXXXXX 200X
DOI: 10.1039/b000000x

SiO_2/Si substrate has been widely used to support two-dimensional (2-D) flakes grown by chemical vapor deposition or prepared by micromechanical cleavage. Raman intensity of the vibration modes of 2-D flakes is used to identify layer number of 2-D flakes on SiO_2/Si substrate, however, such intensity is usually dependent on the flake quality, crystal orientation and laser polarization. Here, we used graphene flakes, a prototype system, to demonstrate how to use the intensity ratio between the Si peak from SiO_2/Si substrates underneath graphene flakes and that from bare SiO_2/Si substrates for layer-number identification of graphene flakes. This technique is robust, fast and nondestructive against sample orientation, laser excitation and presence of defects in the graphene layers. The effect of relevant experimental parameters on the layer-number identification was discussed in detail, such as the thickness of the SiO_2 layer, laser excitation wavelength and numerical aperture of the used objective. This paves the way to use Raman signal from dielectric substrates for layer-number identification of ultrathin flakes of various 2-D materials.

Introduction

Single-layer graphene (SLG) has been regarded as a promising material for its high optical transmittance, low resistivity, high chemical stability and mechanical strength[1,2]. Graphene layers can be stacked to form multilayer graphenes (MLGs) in a hexagonal structure, or, less commonly, in a rhombohedral one. Graphene layers in MLGs are coupled with each other by Van der Waals interaction. We use the notation NLG to indicate MLG with N layers, and thus 10LG means MLG flakes with 10 layers. Additionally, 1LG means SLG. MLGs exhibit many potential applications[3,4] due to their highly tunable electrical properties, such as carrier type or density, rich electronic band structures and various band gaps.[5–7] Therefore, the identification of layer number (N) of NLG flakes is essential to their fundamental study and practical applications. This is true for multilayer flakes of other two-dimensional crystals. There are several techniques to identify N of NLG flakes. Atomic force microscopy (AFM) is a direct and powerful technique to identify N. However, it is time-consuming and not suitable for rapid measurement over large area. Moreover, AFM measurement might be affected by the instrumental offset, substrate roughness and cleanliness of sample surface. Optical contrast is considered as the most powerful characterization tool for NLG flakes, which correlates sample thickness with the contrast of reflection spectra[8–10] or color difference[11–13]. To precisely identify N, the experimental optical contrast must be compared with the theoretical contrast for different N.[10] Optical contrast technique usually can be applied up to N=10 for a given thickness of SiO_2 layer (h_{SiO2}).[8,10]

Raman spectroscopy is one of the most used characterization techniques in carbon science and technology. The Raman spectrum of MLGs consists of the C, D, G and 2D modes. In a MLG comprising N layers, there are N-1 shear (C) modes,[14] where the experimentally-observed C peak with highest frequency is usually denoted as C_{N1}.[7,15] The D mode comes from TO phonons around the Brillouin Zone edge near K, is active by double resonance.[16] The G peak corresponds to the high-frequency E_{2g} phonon at Γ. The 2D peak is the D peak overtone. The D, G and 2D modes are always present in 1LG.[17] The peak parameters of the C, G and 2D modes can be used to identify N of NLG flakes.[14,17–21] By probing the spectral profile of the 2D mode and peak position of the C_{N1} modes, one can determine N of Bernal-stacked NLG flakes up to N=5.[14,20] The peak intensity of the G mode, I(G), of NLG on SiO_2/Si substrate is dependent on N because of the multiple reflection interference within the NLG/SiO_2/Si multilayer.[18,19,21] I(G) will first increase with increasing N and then decrease once N is larger than about 20.[18] The non-monotonicity of I(G) dependent on N makes it difficult to determine N only by I(G). In fact, the Raman peaks of NLG are very sensitive to its doping level, defects and stacking orders.[16] With increasing defects and disorders in NLG, the G and 2D peaks will be weakened in intensity and be broadened in spectral profile. For example, the 2D mode of rhombohedral-stacked 3LG is quite different from that of Bernal-stacked 3LG in lineshape.[22] All these factors will limit the identification of N by the Raman spectrum of

State Key Laboratory of Superlattices and Microstructures, Institute of Semiconductors, Chinese Academy of Sciences, Beijing 100083, China. E-mail: phtan@semi.ac.cn

NLG flakes themselves.[23] Therefore, how to find a universal method to identify N of NLG flakes with defects and different stacking orders up to tens of layer number is still an open and essential issue.

Here, we propose a rapid and efficient technique to identify N of intrinsic and defective NLG flakes, which is applicable for both Bernal-stacked and rhombohedral-stacked NLGs. This technique relies on the variation of Raman mode intensity of the Si peak ($I(Si_G)$) from SiO_2/Si substrate with N of overlying NLG flakes. $I(Si_G)$ decreases monotonically with increasing N of overlying NLG flakes. This trend is dependent on the SiO_2 film thickness, laser excitation wavelength and numerical aperture (NA) of the used objective. The optimized NA is suggested to be less than 0.5. This technique is applicable for NLG over a wide N range up to ($N \sim 100$), which can also be extended for N determination of other two-dimensional materials deposited onto SiO_2/Si substrate.

Experimental details

Highly oriented pyrolytic graphite was mechanically exfoliated on the same Si(110) substrate covered with a 89-nm SiO_2 to obtain NLG flakes.[24] The thickness of NLG flakes was pre-estimated by the AFM measurement with a tapping mode. The NLG flakes with $N < 5$ were determined by Raman spectroscopy via the lineshape of the 2D peak[20], and those with $5 \leq N \leq 10$ were confirmed by optical contrast.[8,10] The instrumental offset (σ) of AFM measurements for 1LG is 1.4nm based on the average of 5 data points.

Raman spectra were measured in back-scattering at room temperature with a Jobin-Yvon HR800 micro-Raman system, equipped with a liquid-nitrogen-cooled CCD, a $\times$100 objective lens (NA=0.90) and a $\times$50 objective lens (NA=0.45). The excitation wavelengths are 633nm from a He-Ne laser and 532nm from a diode-pumped solid-state laser. By monitoring the G peak position[25], we used a laser power of 0.5 mW to avoid sample heating. The resolution of the Raman system is 0.54cm^{-1} (at 532nm) or 0.35cm^{-1} (at 633nm) per CCD pixel. For the Raman measurement of each flake, we focused the laser on the bare substrate close to the graphene flake edge to get a maximum intensity of the Si peak by adjusting the focus of the microscope, measured the Si peak from bare substrate, then moved the laser spot to the graphene flake and measured the Si peak of substrate covered by the graphene flakes and the G peak of the graphene flakes directly. The integration times of 80s and 200s were adopted for the Si and G peaks, respectively, to ensure a good signal-to-noise for both the two peaks.

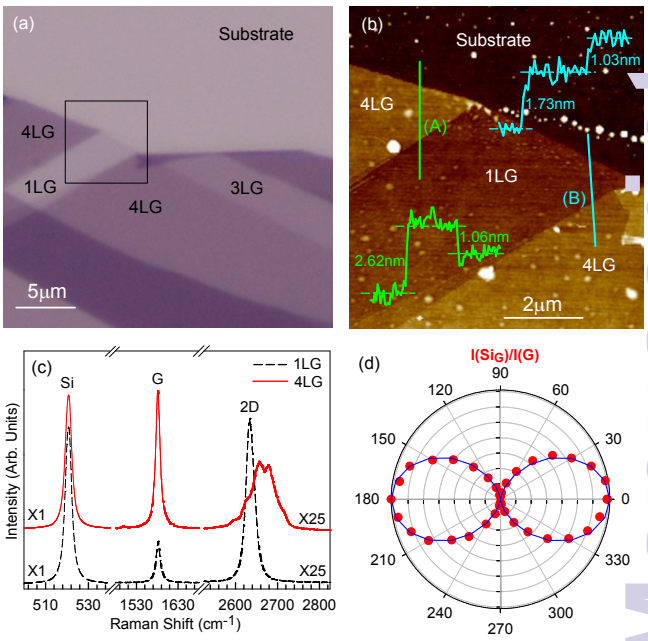

Fig. 1 (a)Optical image of a flake contained 1LG, 3LG and 4LG on a 89-nm SiO_2/Si substrate. (b) AFM image of the sample within the square frame in (a). The height profiles along lines A and B are provided. (c)Raman spectra at 1LG and 4LG regions by 633nm excitation. (d) The intensity ratio between the Si and G peaks at the 4LG region as a function of the excitation laser polarization angle in basal plane by 532nm excitation.

Raman spectra of intrinsic and defective NLG

Fig.1(a) shows the optical image of a flake containing 1LG, 3LG and 4LG on the SiO_2/Si substrate. Fig.1(b) is the AFM image of the black rectangle highlighted in Fig.1(a). The thickness measurements are carried out by two line scans and the corresponding values are also indicated in Fig.1(b). Although the instrumental offset between 1LG and substrate in different measurements may be different, the thickness difference between two flakes stacked together are quite consistent. Raman spectra at the 1LG and 4LG regions are depicted in Fig.1(c) in the spectral range of the Si, G and 2D peaks. 1LG and 4LG can be distinguished by the 2D lineshape. The Si signal is from the SiO_2/Si substrate beneath the 1LG and 4LG flakes, whose peak intensity is denoted as $I(Si_G)$. The Si peak intensity from the bare SiO_2/Si substrate is denoted as $I(Si_0)$. It is clear that $I(Si_G)$ at 4LG is weaker than that at 1LG, while the G band intensity (denoted as I_G) of 4LG is stronger than that of 1LG. $I(G)/I(Si_G)$ has been proposed to count N of graphene flakes.[21] However, we found that this ratio is dependent on the laser wavelength, grating, laser polarization and the orientation of SiO_2/Si substrate. As an example, Fig.1(d) shows the ratio of $I(Si_G)/I(G)$ at 4LG (shown in Fig.1(a)) on 89-nm

SiO_2/Si(110) substrate as a function of the laser polarization angle (θ) in basal plane. Although I(G) is constant for different θ, $I(Si_G) \propto cos^2(\theta)$, sensitive to θ. Thus, it is difficult to identify N of NLG flakes on SiO_2/Si substrate if the substrate is not Si(111).

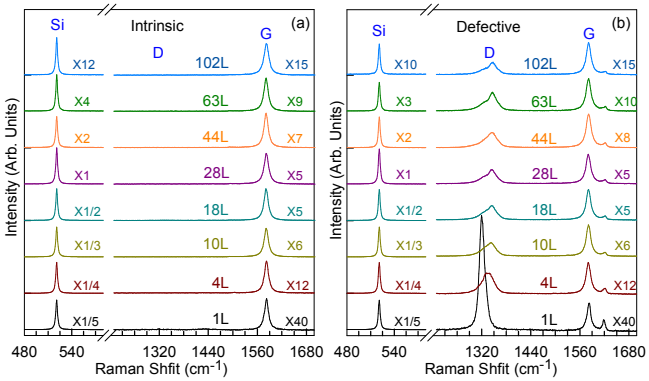

Fig. 2 Raman spectra of intrinsic (a) and defective (b) NLG flakes with specific N in the range of the Si, D and G peaks. N is determined by AFM measurement. The excitation wavelength is 633nm.

$I(Si_0)$ is very strong, usually about 50 times as much as that from bulk graphite. $I(Si_G)$ from substrate beneath NLG flakes is weaker than $I(Si_0)$ because of the absorption of both excitation power to substrate and Si Raman signal from the substrate by the top of graphene flakes. Therefore, in principle, Si Raman signal beneath NLG flakes can be considered to identify N of NLG flakes. In order to fully reveal the experimental conditions for this approach, we prepared 22 intrinsic graphene flakes with different N from 1 to 102 from the AFM measurement. Raman spectra of some graphene flakes are depicted in Fig.2(a) by both objectives with NA of 0.90 and 0.45. The absence of the D mode indicates high crystal quality of these NLG flakes. $I(Si_G)$ decreases and I(G) first increases up to N≈18 and then decreases with increasing N. Considering that the real NLG may be defective, after the above measurement, defects were introduced intentionally for all the NLG flakes by ion implantation. C^+ implantation was performed in an LC-4 type system with the dose and kinetic energy of $2 \times 10^{13}/cm^2$ and $80KeV$, respectively. After the ion implantation, the D peak at $\sim 1350 cm^{-1}$ appears in the Raman spectra of the NLG flakes, as depicted in Fig.2(b), meaning that the NLG flakes become defective. The trend of $I(Si_G)$ and I(G) as a function of N for intrinsic and defective NLG flakes is similar to each other, as shown in Fig.2.

The Si and G peaks at intrinsic and defective NLG flakes were analyzed by the Lorentz fitting. The peak area intensity of the G peak I(G) normalized by $I(Si_0)$ was summarized in Fig.3(a) and the peak area intensity ratio $I(Si_G)/I(G)$ was summarized in Fig.3(b). It clearly shows that $I(G)/I(Si_0)$ reaches

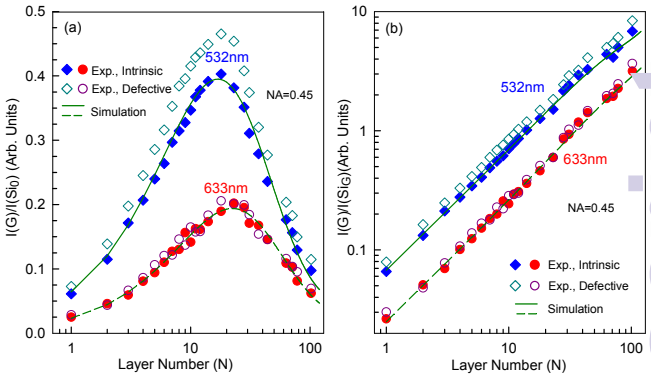

Fig. 3 The experimental and theoretical $I(G)/I(Si_0)$ (a) and $I(G)/I(Si_G)$ (b) as a function of N of NLG flakes. N is determined by AFM measurement. The objective NA is 0.45. The excitation wavelengths of 532nm and 633nm are used.

a maximum at 18LG for laser excitations of both 532 nm and 633 nm. As shown in Fig.3, the experimental $I(G)/I(Si_0)$ and $I(Si_G)/I(G)$ of defective NLG flakes significantly diverge from that of intrinsic NLG flakes. Fig.3(b) shows that $I(Si_G)/I(G)$ decrease monotonically with increasing N. $Log(I(Si_G)/I(G))$ is almost linearly dependent on Log(N). However, in the Raman measurement, we kept the crystal orientation of Si substrate unchanged for all NLG flakes. Once the crystal orientation of substrate is changed or the NLG flake is defected or with disorder, it is impossible to identify N for NLG flakes even for N≤15. New approach based on Raman spectra is necessary for N determination of NLG flakes.

Optical interference model for Raman intensity from multilayer structures

Before exploring new approach for N determination of NLG flakes, we will try to fully understand the behavior of I(G) and $I(Si_G)/I(G)$ as a function of N. Because Raman intensity in multilayer structure is determined by multiple reflection at the interfaces and optical interference within the medium, we adopted the multiple reflection interference method, which has been widely used to quantify optical contrast [8,10,26] and Raman intensities [18,19,21,27] of ultrathin flakes of two-dimensional layered materials. When NLG flakes are deposited on SiO_2/Si substrate, the four layer structure can be established, containing air($\tilde{n}_0$), NLG($\tilde{n}_1, d_1$), $SiO_2(\tilde{n}_2, d_2)$, Si($\tilde{n}_3, d_3$), where $\tilde{n}_i$ and d_i (i=0,1,2,3) are the complex refractive index and the thickness of each medium, as demonstrated in Fig.4.

Similar to previous works [18,19,21,27], to calculate the intensity of Raman signal from the multilayer structures, one must treat the laser excitation and Raman scattering processes separately. As demonstrated in the square frame in Fig.4, the laser intensity profile does not decrease monotonically toward the

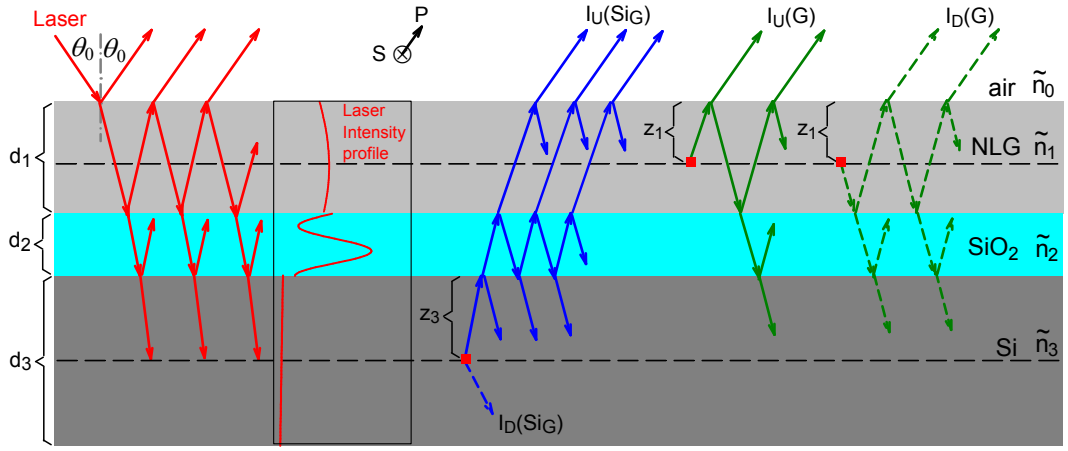

Fig. 4 Schematic diagrams of multiple reflection and optical interference in the multilayer structures containing air, NLG, SiO_2, and Si for the incident laser and out-going Raman signals (the G peak from NLG and the Si peak from Si substrate). $\tilde{n}_0$, $\tilde{n}_1$ (d_1), $\tilde{n}_2$(d_2), and $\tilde{n}_3$(d_3) are the complex refractive indices (thickness) of air, NLG, SiO_2 and Si layers, respectively. The laser intensity distribution along the depth within each medium layer is schematized in the square frame.

Si layer. So, Raman signals from the depth z_1 in the NLG flake and from the depth z_3 in the Si layer will be excited by the laser excitation power at the corresponding depth. The multiple reflection and optical interference are also taken into account in the transition process of Raman signal from the active layers to air. We defined F_L and F_R as respective enhancement factors for laser excitation and Raman signal, similar to the notation of Yoon *et al.*[19,27]. The Raman intensity of a given phonon mode from the medium i can be expressed by integrating over its thickness, d_i, as following equation:

$$I \propto \int_0^{d_i} |F_L(z_i)F_R(z_i)|^2 dz_i. \quad (1)$$

The transfer matrix formalism can be used to calculate F_L and F_R in the multilayer structures, which has been widely used to calculate the Raman signal and optical contrast of NLG flakes on SiO_2/Si substrate.[10,21,26] In order to take the numerical aperture NA of the objective into account, we calculate contributions from each portion of the laser beam by integrating the incident angle θ from 0 to $\arcsin(NA)$. The s-polarization (transverse electric field, $\vec{E}$, perpendicular to the graphene c-axis) and p-polarization (transverse magnetic field, $\vec{H}$, associated to electric field by $\vec{H} = \tilde{n}\vec{E}$) field components[26] are also treated for the transfer matrices. The beam expander is adopted in the optical path to make that the laser beam can be regarded as an ideal parallel beam so that the Gaussian intensity distribution of the incident laser beam is ignored in the calculation. Given that the different polarization dependence of the Raman modes of NLG and substrates due to their different lattice symmetry, the Raman tensor **R** of each phonon mode is also considered. Thus, the total Raman intensity of a Raman mode from the dielectric multilayer is given by integrating over the solid angle (θ, φ for the laser beam and θ', φ' for the Raman signal) of microscope objective and the depth (z_i) in the dielectric layer i:

$$I \propto \int_0^{d_i} \int_0^{\theta'_{max}} \int_0^{2\pi} \int_0^{\theta_{max}} \int_0^{2\pi} \sum_{i=s,p_\perp,p_\parallel} \sum_{j=s',p'_\perp,p'_\parallel} \left| F_L^i(z_i,\theta,\varphi)(\vec{e}_R^{\,j} \cdot \mathbf{R} \cdot \vec{e}_L^{\,i}) F_R^j(z_i,\theta',\varphi') \right|^2 \sin\theta\cos\theta d\theta d\varphi \sin\theta'\cos\theta' d\theta' d\varphi' dz_i, \quad (2)$$

where $\vec{e}_R$ and $\vec{e}_L$ are the electric field vectors of the Raman signal and laser excitation at the depth z_i, respectively. In fact, $I(Si_0)$ can be calculated directly based on the above model once the thickness of graphene flakes is set to zero. Details of calculations of I(G) and $I(Si_G)$ are described in t Supporting Information.

Based on Eq. (2), we calculated I(G) and $I(Si_G)$ as a function of N for NLG flakes on SiO_2/Si(110) substrate. Because d_2 (thickness of SiO_2 layer) is a crucial factor[19] in the analysis of the enhancement factors for the Raman intensity, d_2 is taken as 89 nm measured by a spectroscopic ellipsometer in the calculation. Complex refractive indices of graphene, SiO_2 and Si are considered as the common used ones in previous literatures,[28,29] which is dependent on the wavelength λ. The thickness of 1LG is taken to be 0.335 nm. $I(Si_0)$ was also calculated. The ratio (η) of Raman scattering efficiency between the carbon and silicon atoms is used as an adjustable parameter to fit the experimental $I(G)/I(Si_0)$ and $I(Si_G)/I(G)$ in Fig.3. As depicted in Fig.3, if η is taken as 1.606 for 633nm laser and 0.219 for 532nm laser in this work, the theoretical $I(G)/I(Si_0)$

and I(Si_G)/I(G) are in good agreement with the experimental ones of the intrinsic NLG flakes. One must adjust η to make the theoretical data to fit the experimental one of the defective NLG flakes. It is not applicable in the real practise process for N identification because (1) the prepared NLGs are not always free of defects and (2) the Si substrate used for support each NLG may be random orientation in the chip cutting and in the Raman measurement.

Substrate Raman signal for N identification

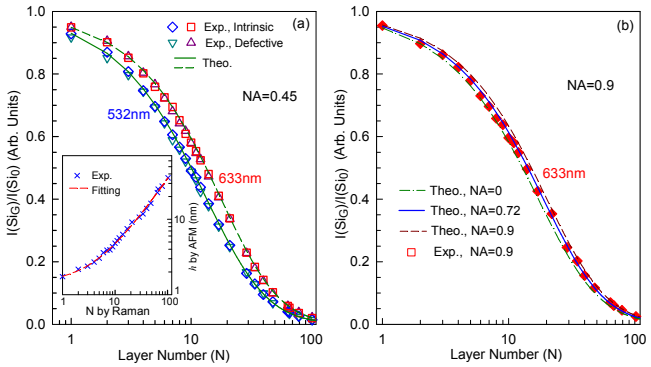

Fig. 5 (a) The theoretical curves and experimental data of I(Si_G)/I(Si_0) for 532-nm and 633-nm excitations and NA=0.45. The thickness of NLG flakes measured by AFM as a function of N identified by Raman measurement are plotted in the inset.(b) I(Si_G)/I(Si_0) as a function of N by the 633-nm excitation for different NA: experimental data (squares, NA=0.9), theoretical curves (lines, NA=0, 0.72, 0.9).

Because the Si peak from SiO_2/Si substrate is much stronger than the G peak from NLG flakes and is hardly modified by the defects or disorders in NLG flakes, the Si peak can be used as a universal peak for N identification of NLG flakes. In order to directly compare the experimental and theoretical data, we calculated I(Si_G)/I(Si_0) as a function of N for two laser excitations of 532nm and 633nm for NA=0.45, as depicted in Fig.5(a) by the solid and dashed lines, respectively. Different excitation wavelengths give different trends for N-dependent I(Si_G)/I(Si_0), however, for both the excitation wavelengths, I(Si_G)/I(Si_0) decreases monotonically with increasing N of NLG flakes. With N increasing from 1 to 10, I(Si_G)/I(Si_0) decreases from $\sim$ 0.95 to $\sim$ 0.55, which is enough for N determination. According to the two theoretical curves, we can determine N of each NLG flake based on the experimental data for each excitation wavelength. We took the round number of the average N determined by 532-nm and 633-nm excitations as the final N for each intrinsic or defective NLG flake. Then, we summarized I(Si_G)/I(Si_0) as a function of N only determined by Raman measurement in Fig.5(a), as shown by diamonds, squares and triangles. Based on this new approach of N identification, the N deviation given by 532-nm and 633-nm excitations is very small, almost zero for N $\leq$ 15, less than 1 for 16$\leq$ N $\leq$ 40, and less than 3 for 41 $\leq$ N $\leq$ 100. N determined by Raman measurement is compared with the thickness (h) of the NLG flakes by AFM measurements, as shown in the inset to Fig.5(a). We used $h = h_0 + d_C N$ to fit the data, giving an AFM offset (h_0) of 1.4 nm and layer spacing distance (d_C) of 0.333 nm. The N deviation between Raman measurement and AFM fitting can be as large as 2 for 21LG, 3 for 34LG and 5 for 66LG.

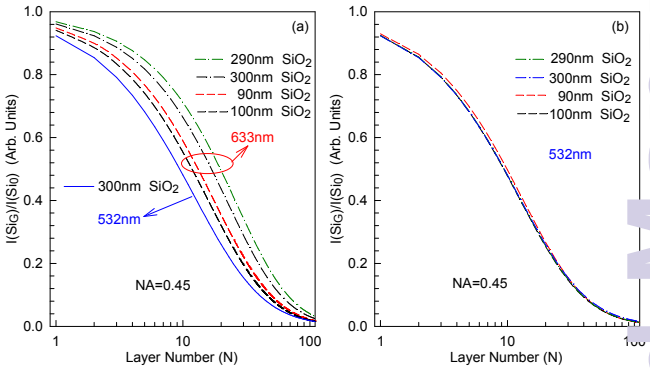

Fig. 6 (a) The calculated I(Si_G)/I(Si_0) excited by a 633-nm excitation as a function of N for different h_{SiO2} and that of h_{SiO2}=300nm excited by a 532-nm excitation for a comparison. (b) The calculated I(Si_G)/I(Si_0) excited by a 532-nm excitation as a function of N for different h_{SiO2}. The NA of the objective is 0.45.

I_{Si_G}/I_{Si_0} was calculated for three NA values of 0, 0.72 and 0.9 excited by the 633-nm excitation, as shown in Fig. 5(b) by dash-dotted, solid and dashed lines, respectively. I_{Si_G}/I_{Si_0} is also dependent on NA. The error of N determination based on theoretical NA=0 for experimental NA=0.9 can be up to 15%. Fig. 5(b) shows I_{Si_G}/I_{Si_0} measured by an objective with NA=0.9, which is found to be consistent with the theoretical one of NA=0.72. The reduction of effective NA in this experiment is similar to the previous reports[10] on the optical contrast of graphene flakes on SiO_2/Si substrate. This reduction can result in an uncertainty of 1 for N<10 and of up to 7 for N=100.

For a purpose of practise application, $I(Si_G)/I(Si_0)$ was calculated for several typical h_{SiO2}. Fig. 6(a) depicts $I(Si_G)/I(Si_0)$ for NLG flakes on the substrate with h_{SiO2}=290nm, 300nm, 90nm and 100nm. It is evident that only a variation of 10 nm for h_{SiO2} can introduce a significant change on the N-dependent curve, which will result in a large error for N determination for a thicker NLG flake. This suggests that precise h_{SiO2} is very important before N determination for NLG flakes on SiO_2/Si substrates by $I(Si_G)/I(Si_0)$, similar to the case of N determination via optical contrast. The difference between

$I(Si_G)/I(Si_0)$ excited by 532-nm and 633-nm excitations for h_{SiO2}=300nm depicted in Fig. 6(a) is more significant than that for h_{SiO2}=89nm as shown in Fig. 5(a). However, for an excitation of 532 nm, the calculated $I(Si_G)/I(Si_0)$ as a function of h_{SiO2} for h_{SiO2}=290nm, 300nm, 90nm and 100nm are almost identical to each other, as demonstrated in Fig. 6(b). The theoretical error for N determination induced by the difference of the four curves can be as small as 1 up to 80LG. Thus, 532-nm excitation is a good option for N determination of NLG flakes on SiO_2/Si substrates once 285nm$< h_{SiO2} <$305nm or 90nm$< h_{SiO2} <$110nm.

The advantages of the N identification based on the Si peak intensity from substrates are summarized here: (1) The Raman intensity from Si substrates can be so intense up to tens of thousands per second that the signal-to-noise of the measured $I(Si_G)/I(Si_0)$ can be very high even for thick graphene flakes. (2) In contrast to $I(Si_G)/I(G)$, this technique does not need to introduce a undetermined Raman efficiency of different atoms in the intensity calculation for the corresponding Raman modes. (3) Because $I(Si_G)$ and $I(Si_0)$ is from the same Si substrate, it makes the measured value $I(Si_G)/I(Si_0)$ robust for any substrate orientation and laser polarization. (4) $I(Si_G)/I(Si_0)$ is not affected by slight disorders as shown in Fig. 5(a) and even doping or adsorption if they do not significantly change the complex refractive index of graphene flakes. (5) The N identification based on Raman spectroscopy offers a high spatial resolution for other optical techniques, such as optical contrast.

There are several factors to be noted in the N identification of NLG flakes based on $I(Si_G)/I(Si_0)$: (1) In order to ensure the accuracy of N identification, a microscope objective with NA$\leq$0.45 is suggested, and smaller effective NA should be considered for larger NA, as shown in Fig.5(b). The reason may be that Raman signal in the entire field of view were not fully collected.[26] (2) h_{SiO2} must be confirmed by initial measurement by a spectroscopic ellipsometer or other techniques because $I(Si_G)/I(Si_0)$ is very sensitive to h_{SiO2}. (3) If the diameter of a laser beam with a Gaussian intensity profile is comparable or smaller than that of the objective aperture, the stronger intensity at the center of the laser beam will result in a smaller effective NA in the theoretical calculation to fit the experimental results.

Conclusions

We demonstrated a robust, fast and nondestructive method to identify the layer number of graphene flakes on SiO_2/Si substrates for any substrate orientation and laser polarization. The intensity ratio of the Si peak from SiO_2/Si substrates underneath graphene flakes to that from bare SiO_2/Si substrates is used as a probe for the layer number. The high signal-to-noise of the ratio make this method robust against presence of defects in the graphene layers. This technique can be extended for layer-number identification of ultrathin flakes of other two-dimensional materials, such as semimetals ($NiTe_2$ and VSe_2), semiconductors (WS_2, WSe_2, MoS_2, $MoSe_2$, $MoTe_2$, TaS_2, $RhTe_2$ and $PdTe_2$), insulators (HfS_2), superconductors (NbS_2, $NbSe_2$,$NbTe_2$, and $TaSe_2$) and topological insulators (Bi_2S_3 and Bi_2Te_3).[30]

Acknowledgments

We acknowledge support from the National Natural Science Foundation of China, grants 11225421, 11434010 and 114742[illegible].

References

1 A. K. Geim and K. S. Novoselov, *Nature Materials*, 2007, **6**, 183.
2 F. Bonaccorso, Z. Sun, T. Hasan and A. C. Ferrari, *Nature Photonicsm* 2010, **4**, 611.
3 J. B. Oostinga, H. B. Heersche, X. Liu, A. F. Morpurgo and L. M. Vandersypen, *Nature Materials*, 2008, **7**, 151.
4 M. F. Craciun, S. Russo, M. Yamamoto, J. B. Oostinga, A. F. Morpu[illegible] and S. Tarucha, *Nature Nanotechnology*, 2009, **4**, 383.
5 B. Partoens and F. M. Peeters, *Phys. Rev. B*, 2006, **74**, 075404.
6 A. Grueneis, C. Attaccalite, L. Wirtz, H. Shiozawa, R. Saito, T. Pichler and A. Rubio, *Phys. Rev. B*, 2008, **78**, 205425.
7 J.-B. Wu, X. Zhang, M. Ijäs, W.-P. Han, X.-F. Qiao, X.-L. Li, D.-S. Jiang, A. C. Ferrari and P.-H. Tan, *Nat. Commun.*, 2014, **5**, 5309.
8 Z. H. Ni, H. M. Wang, J. Kasim, H. M. Fan, T. Yu, Y. H. Wu, Y. P. Feng and Z. X. Shen, *Nano Letters*, 2007, **7**, 2758.
9 P. Blake, E. W. Hill, A. H. C. Neto, K. S. Novoselov, D. Jiang, R. Yang, T. J. Booth and A. K. Geim, *Appl. Phys. Lett.*, 2007, **91**, 063124.
10 W. P. Han, Y. M. Shi, X. L. Li, S. Q. Luo, Y. Lu and P. H. Tan, *Acta Phys. Sin.*, 2013, **62**, 110702.
11 L. Gao, W. Ren, F. Li and H.-M. Cheng, *ACS Nano*, 2008, **2**, 1625.
12 H. Li, J. Wu, X. Huang, G. Lu, J. Yang, X. Lu, Q. Zhang and H. Zhang, *ACS Nano*, 2013, **7**, 10344.
13 Y.-F. Chen, D. Liu, Z.-G. Wang, P.-J. Li, X. Hao, K. Cheng, Y. Fu, L.-X. Huang, X.-Z. Liu and W.-L. Zhang, *Journal of Physical Chemistry C* 2011, **115**, 6690.
14 P. H. Tan, W. P. Han, W. J. Zhao, Z. H. Wu, K. Chang, H. Wang, Y. F. Wang, N. Bonini, N. Marzari, N. Pugno, G. Savini, A. Lombardo [illegible] A. C. Ferrari, *Nature materials*, 2012, **11**, 294.
15 P.-H. Tan, J.-B. Wu, W.-P. Han, W.-J. Zhao, X. Zhang, H. Wang and Y.-F. Wang, *Phys. Rev. B*, 2014, **89**, 235404.
16 A. C. Ferrari and D. M. Basko, *Nat. Nanotech.*, 2013, **8**, 235–246.
17 A. C. Ferrari, J. C. Meyer, V. Scardaci, C. Casiraghi, M. Lazzeri, F. Mauri, S. Piscanec, D. Jiang, K. S. Novoselov, S. Roth and A. K. Geim, *Phys. Rev. Lett.*, 2006, **97**, 187401.
18 Y. Y. Wang, Z. H. Ni, Z. X. Shen, H. M. Wang and Y. H. Wu, *Appl. Phys. Lett.*, 2008, **92**, 043121.
19 D. Yoon, H. Moon, Y.-W. Son, J. S. Choi, B. H. Park, Y. H. Cha, Y. D. Kim and H. Cheong, *Phys. Rev. B*, 2009, **80**, 125422.
20 W. J. Zhao, P. H. Tan, J. Zhang and J. Liu, *Phys. Rev. B*, 2010, **82**, 245423
21 Y. K. Koh, M.-H. Bae, D. G. Cahill and E. Pop, *ACS Nano*, 2011, **5**, 269.
22 C. H. Lui, Z. Li, Z. Chen, P. V. Klimov, L. E. Brus and T. F. Heinz, *Nano Lett.*, 2011, **11**, 164–169.
23 A. C. Ferrari, *Solid State Commun.*, 2007, **143**, 47.
24 K. S. Novoselov, D. Jiang, T. Booth, V. V. Khotkevich, S. M. Morozov and A. K. Geim, *Proc. Natl. Acad. Sci. U.S.A.*, 2005, **102**, 10451.

25 P. Tan, Y. Deng, Q. Zhao and W. Cheng, *Appl. Phys. Lett.*, 1999, **74**, 1818–1820.
26 C. Casiraghi, A. Hartschuh, E. Lidorikis, H. Qian, H. Harutyunyan, T. Gokus, K. S. Novoselov and A. C. Ferrari, *Nano Letters*, 2007, **7**, 2711.
27 S.-L. Li, H. Miyazaki, H. Song, H. Kuramochi, S. Nakaharai and K. Tsukagoshi, *ACS Nano*, 2012, **6**, 7381.
28 V. G. Kravets, A. N. Grigorenko, R. R. Nair, P. Blake, S. Anissimova, K. S. Novoselov and A. K. Geim, *Phys. Rev. B*, 2010, **81**, 155413.
29 E. D. Palik, *Handbook of Optical Constants of Solids*, Academic Pre. New York, 1985.
30 A. K. Geim and I. V. Grigorieva, *Nature*, 2013, **499**, 419.

The table of contents entry Raman signal from Si substrate has been used as a robust, fast and nondestructive way to probe the layer number of graphene flakes up to 100 layers.

ToC figure